Biogeosciences Discuss., doi:10.5194/bg-2017-11, 2017
Manuscript under review for journal Biogeosciences
Published: 18 January 2017

Biogeosciences Discussions Open Access EGU

Patterns and controls of inter-annual variability in the terrestrial Carbon budget

Barbara Marcolla[1], Christian Rödenbeck [2], Alessandro Cescatti [3]

[1]Fondazione Edmund Mach, IASMA Research and Innovation Centre, Sustainable Agro-ecosystems and Bioresources Department,38010 San Michele all'Adige, Trento, Italy
[2]Max Planck Institute for Biogeochemistry, 07745 Jena, Germany.
[3]European Commission, Joint Research Centre, Directorate for Sustainable Resources, I-21027 Ispra (VA), Italy

Correspondence to: Alessandro Cescatti (alessandro.cescatti@ec.europa.eu)

Abstract. The terrestrial carbon fluxes show the largest variability among the components of the global carbon cycle and drive most of the temporal variations in the growth rate of atmospheric CO_2 (Le Quéré 2014). Understanding the environmental controls and trends of the terrestrial carbon budget is therefore essential to predict the future trajectories of the CO_2 airborne fraction and atmospheric concentrations. In the present work, patterns and controls of the inter-annual variability (IAV) of carbon Net Ecosystem Exchange (NEE) have been analysed using three different data-streams: ecosystem level observations from the FLUXNET database (La Thuille and 2015 releases), the MPI-MTE bottom-up product resulting from the global up-scaling of site-level fluxes, and the Jena CarboScope Inversion, a top-down estimate of surface fluxes obtained from observed CO_2 concentrations and an atmospheric transport model. Consistencies and discrepancies in the temporal and spatial patterns and in the climatic and physiological controls of IAV were investigated between the three data sources. The global average of IAV at FLUXNET sites (~120 gC m^{-2} y^{-1}), quantified as the standard deviation of annual NEE, was observed to peak in arid ecosystems and to be almost six times larger than the values calculated from the two global products (15 and 20 gC m^{-2} y^{-1} for MPI-MTE and Jena inversion, respectively). The two data-driven global products show that most of the temporal variability observed in the last three decades is due to yearly anomalies, whereas the temporal trends explain only about 15% of the variability in the MPI-MTE product and 20% in the Jena Inversion product. Both at site level and at global scale, the IAV of NEE is driven by the gross primary productivity and in particular by the cumulative carbon flux during the months when land acts as a sink. Altogether these results offer a broad view on the magnitude, spatial patterns and environmental drivers of IAV from a variety of data sources, that can be instrumental to improve our understanding of the terrestrial carbon budget and to validate the predictions of land surface models.

1 Introduction

Atmospheric CO_2 concentration has been constantly increasing since the Industrial Revolution, and has caused a corresponding rise of 0.85 °C in the global air temperature from 1880 to 2012 (IPCC, 2013). Since the 1960s, terrestrial ecosystems have acted as a considerable sink for atmospheric CO_2, reabsorbing about one quarter of anthropogenic emissions (Friedlingstein et al., 2010; Le Quéré et al., 2014). The growth rate of atmospheric CO_2 concentration is characterized by a large inter-annual variability (IAV), which mostly results from the variability of the CO_2 net ecosystem exchange (NEE) on land (Bousquet et al., 2000; Le Quere et al., 2009; Yuan et al., 2009). Multisite synthesis confirms that a large inter-annual variability in NEE is a common feature at all flux sites around the world (Baldocchi, 2008; Baldocchi et al., 2001). The reason why the IAV is so large is that NEE results from the small imbalance between two larger fluxes: the photosynthetic uptake of CO_2 (Gross Primary Production, GPP) and the respiratory release of CO_2 (Total Ecosystem Respiration, TER). As a consequence, even minor variation in either of the two fluxes can cause large variations in their difference.

Biogeosciences Discuss., doi:10.5194/bg-2017-11, 2017
Manuscript under review for journal Biogeosciences
Published: 18 January 2017

It has been long debated which of GPP or TER controls the spatial and temporal variability of NEE. Several studies have ascribed inter-annual variability in NEE to variability in either GPP (Ahlstrom et al., 2015; Janssens et al., 2001; Jung et al., 2011, 2017; Stoy et al., 2009; Urbanski et al., 2007) or TER (Morgenstern et al., 2004; Valentini et al., 2000) or both (Ma et al., 2007; Wohlfahrt et al., 2008b). GPP and TER show comparable ranges of IAV, typically larger in absolute terms than that observed for NEE due to the temporal correlation between the two gross fluxes (Richardson et al., 2007). Given that photosynthesis and respiration may respond differently to environmental drivers (Luyssaert et al., 2007; Polley et al., 2008), the interpretation of climate impacts on the variability of NEE requires the understanding of the relation between the IAV of NEE and that of GPP and TER (Polley et al., 2010).

The environmental factors driving the IAV of NEE (IAV_{NEE}) include: climate, physiology, phenology, natural and anthropogenic disturbances (Marcolla et al., 2011; Richardson et al., 2007; Shao et al., 2015). Understanding the spatio-temporal variability of NEE and its controlling mechanisms is essential to assess the vulnerability of the terrestrial carbon budget, to evaluate the land mitigation potentials and to quantify the ecosystem capacity to store carbon under future climatic conditions (Heimann and Reichstein, 2008). Besides, quantifying inter-annual variability in NEE is a prerequisite for detecting longer-term trends or step changes in flux magnitude in response to climatic or anthropogenic influences and identifying its drivers (Cox et al., 2000; Lombardozzi et al., 2014).

The temporal dynamic of NEE has been addressed in numerous studies, based on either ‘‘top-down’’ approaches, which primarily focuses on aircraft atmospheric budgets (Leuning et al., 2004), tower based boundary layer observations (Bakwin et al., 2004) and tracer transport inversion (Baker et al., 2006; Gurney et al., 2002; Rödenbeck et al., 2003), or on ‘‘bottom-up’’ methods that rely on data-driven gridded products derived from the up-scaling of flux data (Jung et al., 2011, 2017; Papale et al., 2015; Papale and Valentini, 2003) or process-based biogeochemical models that simulate regional carbon budgets (Desai et al., 2008, 2007; Mahadevan et al., 2008).

Despite the broad literature on the subject, very few examples of IAV analysis based on multiple data streams are available in the literature (Desai et al., 2010; Pacala, 2001; Poulter et al., 2014). In the present study patterns and controls of the inter-annual variability of NEE have been analysed using three different data streams: ecosystem level data from the FLUXNET database, the MPI-MTE bottom-up product resulting from the statistical up-scaling of in-situ flux data (Jung et al., 2009) and the Jena CarboScope Inversion top-down product, which estimates land (and ocean) fluxes from atmospheric CO_2 concentration measurements and atmospheric transport modelling (Rödenbeck et al., 2003). In particular, this analysis aims to: i) assess the magnitude and the spatial pattern of IAV of NEE (IAV_{NEE}), ii) identify the role of photosynthesis and respiration as sources of IAV_{NEE} and iii) investigate the role of key climatic variables like temperature and precipitation in driving the spatial pattern of IAV. Finally, the consistencies and discrepancies among the different data products are analysed and critically evaluated.

2 Materials and Methods

2.1 Datasets

Data at ecosystem scale were retrieved from two releases of the FLUXNET dataset, namely LaThuile and 2015. These datasets contain half-hourly data of carbon dioxide, water vapour and energy fluxes that are harmonized, standardized and gap-filled. Time series of NEE and of the component fluxes GPP and TER, together with air temperature and precipitation, were used in the present analysis. Flux data have the advantage to represent direct observations of in-situ IAV, however at most sites the time series are still too short for a proper analysis of the temporal variability of NEE (Shao et al., 2015). For this reason only sites with a minimum of five years of observations and an open data distribution policy were selected. A subset of 89 sites satisfied the two criteria, among which 27 evergreen needle-leaf forests (ENF), 5 Evergreen Broadleaf Forests (EBF), 12 deciduous broad-leaf forests (DBF), 6 mixed forests (MF), 12 grasslands (GRA), 8 croplands (CRO), 6

Biogeosciences Discuss., doi:10.5194/bg-2017-11, 2017
Manuscript under review for journal Biogeosciences
Published: 18 January 2017

sites counting closed and open shrublands (CSH, OSH), 7 wetlands (WET) and 6 sites counting savannas and woody savannas (SAV, WSA).

At global scale, two sources of gridded data were used: a "bottom-up" data product, namely the MPI-MTE product (Jung et al., 2009) and, as "top-down" product, the Jena CarboScope CO_2 Inversion (Rödenbeck et al., 2003). The MPI-MTE dataset is built with a machine learning technique (model tree ensemble, MTE) to upscale in space and time the flux observations from the global network of eddy covariance sites (FLUXNET) integrated with climate and remote sensing data for the time period 1982-2011 (Jung et al., 2009). Effects of land management, land use change and CO_2 fertilization are not represented in this product. Global maps for GPP and TER at 0.5° spatial resolution and monthly temporal resolution were used, while NEE fields were calculated as difference between the gross fluxes. To derive surface fluxes, the Jena CarboScope Inversion combines modelled atmospheric transport with high-precision measurements of atmospheric CO_2 concentrations. Atmospheric transport is simulated by a global three-dimensional transport model driven by meteorological data. For consistency with the MPI-MTE product, monthly averaged NEE land fluxes from the s81_v3.6 version of the product were used here, at a spatial resolution of 5° x 3.75°. The Jena Inversion is particularly suited for the analysis of temporal trends and variability since it is based on a temporally constant observation network (14 atmospheric stations for the version s81_v3.6).

As the inversion estimates the total land flux, it includes CO_2 emissions from fires in addition to NEE, being calculated as the difference between the total surface flux and prescribed anthropogenic emissions. For improving the consistency of the two datasets, we therefore subtracted fire emissions from the inversion estimates using an harmonized combination of the products RETRO (Schultz et al., 2008) for the period 1982-1996 and GFED4 (Van Der Werf et al., 2010) for the period 1997-2013. RETRO is a global gridded data sets (at 0.5° spatial resolution) for anthropogenic and vegetation fire emissions of several trace gases, covering the period from 1960 to 2000 with monthly time resolution. GFED4 combines satellite information on fire activity and vegetation productivity to estimate gridded monthly fire emissions at a spatial resolution of 0.25 degrees since 1997. RETRO and GFED4 were harmonized using the overlapping years (1997-2000) to calculate calibration coefficients as the ratio of GFED4 to RETRO for latitudinal bands of 30°. The RETRO time series was then multiplied by these coefficients and the resulting time series of fire emissions was finally subtracted from the land flux of the Jena Inversion. It is worth noting that the remaining flux from the inversion is the sum of land use change emissions and NEE while the MPI-MTE does not account for the land use change flux.

In order to analyse the role of climatic drivers on the inter-annual variability, global maps of temperature and precipitation were used. Gridded Air temperatures were obtained from the Climatic Research Unit (CRU) at the University of East Anglia at monthly time scale and 0.5°x0.5° spatial resolution, based on an archive of monthly mean temperatures provided by more than 4000 weather stations (Jones et al., 2012). Precipitation fields were obtained from the GPCC product at 0.5° and monthly time step (Schneider et al., 2014) . This product is based on a large dataset of monthly precipitation from more than 85,000 stations and is provided by NOAA/ESRL PSD (Boulder, Colorado, USA). The MODIS MCD12C1 land cover product (Friedl and Brodley, 1997) was used to classify the land pixels and to calculate statistics by plant functional type. MCD12C1 provides the dominant land cover types at a spatial resolution of 0.05° using a supervised classification algorithm that is calibrated using a database of land cover training sites.

2.2 IAV Analysis

The inter-annual variability of NEE was estimated as the standard deviation of annual values computed on time windows of 12 months shifted with a monthly time step (Shao et al., 2015; Yuan et al., 2009) and calculated with the same methodology for the three data-streams used in the analysis. Average values of IAV for plant functional type (PFT) were determined using the PFT classification of FLUXNET sites and the MCD12C1 product (aggregated at the appropriate spatial resolution using the dominant PFT) for the MPI-MTE and Jena Inversion.

Biogeosciences Discuss., doi:10.5194/bg-2017-11, 2017
Manuscript under review for journal Biogeosciences
Published: 18 January 2017

For the two gridded products, which provide a 30 year long time series (1982-2011), the IAV was partitioned in two components, namely the variance explained by the temporal trend and that due to annual anomalies (Ahlstrom et al., 2015). For this purpose a linear model was fitted on the time series at each pixel, and the determination coefficient of the regression was used to measure the fraction of variance explained by the trend, whereas its complement to one was the fraction of variance due to anomalies.

The spatial correlation between IAV and climatic drivers (air temperature and precipitation) was analysed at global scale by calculating the spatial correlation coefficient between the temporal standard deviation (IAV amplitude) of NEE and the average annual temperature or precipitation in moving spatial windows of 15°x11.5° (which means 31x21 pixels for MPI-MTE). The latitudinal averages of these correlation coefficients were calculated for latitudinal bands of 30°.

Finally, in order to identify which process between photosynthesis and respiration drives IAV_{NEE}, for FLUXNET and MPI-MTE linear regressions between NEE and GPP or TER were fitted and the difference between the two determination coefficients was computed. Since GPP and TER cannot be derived from inversion products, we performed a similar analysis using NEE of the Carbon Uptake Period (CUP, sum of negative monthly NEEs) and of the Carbon Release Period (CRP, sum of positive monthly NEE), as proxies of GPP and TER for all the three data streams. Finally, IAV_{NEE} and IAV controls were also analysed in a climatic space defined by mean annual temperature and precipitation.

3 Results and Discussion

3.1 IAV patterns

Figure 1 shows the spatial pattern of inter-annual variability for the three data sets. The IAV of NEE at individual Fluxnet sites ranges from 15 to 400 gC $m^{-2}y^{-1}$ and shows an average of 130 gC $m^{-2}y^{-1}$. On average the most northern sites show a lower temporal variability both in Europe and in North America (Fig. 1a). A global map of IAV_{NEE} is shown also for MPI-MTE (Fig. 1b) and Jena Inversion (Fig. 1c) at the original spatial resolutions of the two products. The observed range of IAV is similar for the two gridded products and substantially lower than that observed at site level, probably due to the spatial averaging of the land fluxes that dampens the temporal variability. The mean global value of IAV is in fact 15 and 20 gC m^{-2} y^{-1} for MPI-MTE and Jena Inversion, respectively, and hence about one sixth of the site level IAV. The two gridded products confirm the decreasing trend of IAV toward northern latitudes observed at flux sites. A general decrease of IAV_{NEE} at higher latitude for both ENF and DBF was also observed by Yuan et al. (2009) although for none of the two PFTs these trends were significant.

In terms of IAV, the two global products show a reasonable qualitative correspondence for North America and Eurasia, whereas they disagree for South America, with MPI-MTE showing a minimum of IAV in the humid Tropics, where the inversion product shows on the contrary a high variability. MPI-MTE in particular shows maximum values along the Eastern coast of South America while the Jena Inversion shows an almost opposite pattern. A similar behaviour is observed also in Africa, where the top-down product shows a maximum in central Africa while MPI-MTE shows a minimum in the Congo basin and higher values in arid zones like Sahel and South Africa. These discrepancies could, on the one hand, be ascribed to the limits of the bottom-up approach in dealing with the low seasonality of the fraction of absorbed radiation (FaPAR) in evergreen broadleaf forests, given the relevance of this predictor in the MPI-MTE estimates. A second reason for the discrepancy could be due to the CO_2 emissions from land use change that is particular relevant in some tropical areas but are not accounted in the MPI-MTE estimates. On the other hand, the fine-scale estimates of the inversion are largely determined by the a-priori weighting pattern, which has been chosen proportional to time-mean NPP (from the LPJ model) as a vegetation proxy (Rödenbeck et al., 2003). As the atmospheric data can only constrain larger-scale patterns comparable to the distances between the stations, this means that IAV will be locally higher where mean NPP is high, and vice versa.

Biogeosciences Discuss., doi:10.5194/bg-2017-11, 2017
Manuscript under review for journal Biogeosciences
Published: 18 January 2017

As far as the Northern Hemisphere is concerned, a good correspondence is observed in western Eurasia, while some discrepancies are observed in other zones; for example MPI-MTE shows a large IAV in India, probably driven by the changes in FaPAR related to agricultural intensification, which is not emerging from the inversion product that has little observational constraint in this area. To summarize, the spatial pattern of IAV in the two products better agrees in the Northern Hemisphere for temperate and cold temperate zones, whereas for the southern Hemisphere, and in particular for the humid evergreen forests, they show a poor match. In general it has to be considered that both the MPI-MTE product and the Jena inversion are driven by data from surface networks that are very sparse in the Tropics and Southern Hemisphere and, therefore, these observation-driven estimates are under-constrained in those areas. The results presented in the maps of Figure 1 are summarized in the climate space in Figure 2. Map pixels were classified according to mean annual temperature and precipitation, and the mean value of IAV_{NEE} and normalized IAV_{NEE} were calculated for each climate bin.

Given that the standard deviation of NEE increases with the primary productivity at the Fluxnet sites (Figure 3), we normalized IAV of both MPI-MTE and Jena inversion by the average GPP of the specific climate bin from the MPI-MTE. The normalized IAV shows a decreasing trend at increasing temperature and precipitation, which means that arid ecosystems show a higher variability in both data products, in accordance with previous findings (Ahlstrom et al., 2015). In terms of absolute IAV, MPI-MTE shows the highest IAV at high temperature and intermediate precipitation levels, whereas Jena Inversion has its maximum in warm humid classes.

The dependency of IAV_{NEE} on GPP and on NEE_{CUP} is reported in Figure 3 for the three datasets. Both for Fluxnet and the Jena Inversion, IAV is positively related to either GPP or NEE_{CUP}. On the contrary, the IAV_{NEE} in the MPI-MTE dataset peaks at intermediate values of GPP and NEE_{CUP}, even if this trend is not evident in the Fluxnet data from which the MPI-MTE product is derived. As stressed previously, this latter product seems to underestimate the temporal variability of evergreen tropical forests both in South America and Africa, where the highest values of GPP and NEE_{CUP} are observed and where on the contrary the inversion shows high values of IAV.

Figure 4 shows the dependence of IAV_{NEE} on the spatial resolution of the analysis for both global products (i.e. MPI-MTE and Jena Inversion) to verify if and to which extend the spatial scale is responsible for the differences observed between them. The two products show a good agreement at the native Inversion resolution (5°x3.75°) and at global level when only one global value is retrieved, spatially averaging all the pixels of the original maps. For the MPI-MTE product, the observed IAV is decreasing regularly at decreasing map resolution. On the contrary, the Jena Inversion shows a rapid descent followed by a stabilisation, probably due to a larger spatial coherence of the inversion signal compared to the MTE product.

The fractions of IAV_{NEE} generated either by temporal trends or by annual anomalies are summarized in Fig. 5 for the two global gridded products. For MPI-MTE, more than 80% of the IAV is explained by anomalies at all latitudes. Only in limited zones like Congo and Western Amazonia, MPI-MTE shows a relative minimum in the importance of anomalies, but this global product might underestimate the total variability in these zones (see Fig. 1b). Anomalies explain the largest share (between 62 and 90%, average 77%) of the temporal variability also in the Jena Inversion, with a higher relevance of trends in the southern hemisphere. The inversion product shows several hotspots of trend-driven variability, like south Africa, south America and northern Eurasia that is indeed reported as an area or increasing productivity in the last decades. In the interpretation of these results it is important to consider that MPI-MTE is generated by the statistical upscaling of Fluxnet data, using climate and FaPAR as predictors. This methodology relies on the assumption of a constant ecosystem response to climate drivers and for this reason the product cannot reproduce the influence of environmental factors (e.g. increasing CO_2 concentration or nitrogen deposition) that alter these responses but are not reflected in input variables like FaPAR. On the contrary, inversion products do not make any assumption on the climate dependence of ecosystem functioning, but include also emission from land management and land use change that may hide or emphasize the NEE trends. In summary, it is important to notice that, despite the important climate trends, in the last 30 years the temporal variability of the land carbon

Biogeosciences Discuss., doi:10.5194/bg-2017-11, 2017
Manuscript under review for journal Biogeosciences
Published: 18 January 2017

205 balance has been driven by annual anomalies, confirming the dominant role of climate variability on the terrestrial C budget (Le Quéré et al., 2014).

For the two gridded products the analysis of IAV (either in terms of absolute IAV_{NEE} or normalized with NEE_{CUP}) was disaggregated by plant functional type (Figure 6). The analysis in terms of absolute IAV_{NEE} shows that savannas and woody savannas (WSAV-SAV) are the PFTs characterized by the larger IAV and variability within the PFT. This was found both
210 for the MPI-MTE and the Jena Inversion product and confirms the results of a recent study (Ahlstrom et al., 2015) in which semi-arid ecosystems were found to account for the largest fraction (39%) of the global IAV in net biome productivity. This variability was found to be significantly related to the length of the growing season (Ma et al., 2007). In terms of normalized IAV the two gridded products show different behaviours, CSH-OSH being the most variable PFT for MPI-MTE while the inversion data report a higher variability for EBF and WSAV-SAV. As observed at pixel scale in Figure 1, even at PFT level
215 the results obtained from Fluxnet sites show a higher variability than the gridded products. In general at Fluxnet sites IAV is proportional to ecosystem productivity (Fig 4) with the maximum values observed in EBF, DBF-MF and CRO-GRA and the minimum in WET. The large value of IAV observed in GRA-CRO is presumably also affected by the potential large impact of management in these ecosystems that can either reduce (e.g. by irrigation) or increase the climate-induced variability (e.g. by changing crops or fertilization schemes, etc.).

220 **3.2 Climate dependence of IAV**

The climatic dependence of the spatial variability of IAV_{NEE} at global scale for the MPI-MTE product (Figure 7) shows a clear pattern with positive correlations in temperature-limited areas at northern latitudes, and negative temperature dependence in water-limited zones (Braswell et al., 1997). These observations agree with Reichstein et al. (2007), which report that GPP shifts from soil water content to air temperature dependency at around 52° N. These opposite temperature
225 dependences will probably lead to future contrasting changes in IAV. In fact, under a global warming scenario, the northern latitudes will be characterized by a larger sink (Zhao and Running, 2010) but also by a larger temporal variability, while arid zones like the Mediterranean basin, the Middle East Australia and the Sub-Saharan Africa will probably experience a reduction in IAV linked to large-scale droughts and consequent reduction in primary productivity (Ciais et al., 2005). Concerning precipitation the MPI-MTE product show more complex spatial patterns with negative correlation in the humid
230 tropics, temperate Europe and South-East USA and positive correlation elsewhere.

The climate dependencies of IAV are further separated between the variability due to trends and anomalies (Fig. 8, Fig. 2). The two components of IAV_{NEE} mostly show an agreement in the sign of the climatic controls, meaning that the environmental drivers have the same effects on trends and anomalies, and therefore support the use of IAV to investigate long term climatic responses. An exception to this pattern is represented by the correlation with precipitation retrieved from
235 MPI-MTE, which shows an unclear latitudinal pattern. In general anomalies show a higher correlation than trends, probably due to the larger magnitude of the variance attributed to this component. In conclusion, the spatial patterns shown in the maps of Fig. 7 and the agreement between the two components of IAV reported in the barplots indicate that the temperature controls of IAV of NEE is in general the same as for the primary productivity (i.e. positive in colder biomes and negative in warmer regions), while the contrasting results observed for precipitation suggest that the role played by water availability on
240 the spatial and temporal variability is unclear, probably because of the temporal correlation between precipitation and temperature anomalies, as shows by Jung et al. (2017). The analysis of the climate drivers of IAV was not performed for the Jena inversion because for this product local variation in IAV are heavily driven by the prior estimates of NPP and therefore results have limited sensitivity to the atmospheric constraints.

Biogeosciences Discuss., doi:10.5194/bg-2017-11, 2017
Manuscript under review for journal Biogeosciences
Published: 18 January 2017

3.3 Physiological drivers of IAV

An improvement in the mechanistic understanding of IAV_{NEE} can be achieved by partitioning the net flux in its two components: GPP and TER. Partitioned fluxes are available for Fluxnet sites and for derived products like MPI-MTE, while they cannot be derived from atmospheric inversions. For this latter product the fluxes during the Carbon Uptake Period (CUP; NEE<0) and during the Carbon Release Period (CRP; NEE>0) were used in this analysis as proxies of GPP and TER, respectively.

To investigate how good this proxy is, the ratios TER/GPP during CUP and GPP/TER during CRP were analysed at Fluxnet sites and for each pixel of the MPI-MTE product and averaged by PFT (Figure 8a). As far as the MPI-MTE product is concerned, TER ranges from 55 to 78% of GPP during the CUP while GPP is 56 to 80% of TER during the CRP, hence on average about two-thirds of the signal come from GPP (TER) in the CUP (CRP). These ratios show a certain variability among PFTs, with ENF having the larger imbalance between the two fluxes and the lowest ratio TER/GPP during CUP (due to the strong seasonality of GPP in this PFT), while the two fluxes are not so well partitioned for EBFs (ratio ~0.8) that are characterized by a long growing season with consistently large fluxes of GPP and TER. The other PFTs show an average ratio value of ~0.65 both in CUP and CRP. In summary, it can be inferred that NEE during CUP is dominated by the signal of GPP, while NEE during CRP is dominated by TER even though to a smaller extent, as it emerges from the frequency distributions in Figure 8bc calculated from the MPI-MTE product. The distribution of the ratio TER/GPP during the CUP is in fact narrower and peaks at a value of 0.7, while a broader distribution is observed for the GPP/TER ratio during the CRP. As expected there is a larger spread in the composition of NEE during CRP across the World, and this is linked to the larger variability in the seasonality of GPP that may actually go to zero in the dormancy season, while TER is always positive.

In order to identify which of the gross fluxes controls the variability of the net land flux, linear regressions were fitted on the NEE time series of each pixel/site against GPP or TER and CUP or CRP. The difference between the variance explained by the two flux components (difference of the determination coefficients of the two regressions, where statistically significant) was used to determine which component (GPP vs TER or NEE_{CUP} vs NEE_{CRP}) drives the inter-annual variation of NEE. Figure 9a shows that, in most of the land area, the IAV_{NEE} is driven by GPP both at Fluxnet sites and for the MPI-MTE product. The same data products show an even clearer dominance of NEE_{CUP} in the IAV (Fig. 9b). The Jena Inversion product shows that, although most of the globe is NEE_{CUP} driven, there are quite a few areas that are weakly CRP driven like eastern US, arid regions in Africa and the Amazon basin, probably because these areas are estimated to be CO_2 sources in this inversion and therefore NEE is dominated by NEE_{CRP} (data not shown). When latitudinal profiles are considered, all the products show that GPP and NEE_{CUP} dominate the temporal variability of yearly NEE more than TER or NEE_{CRP} (le Maire et al., 2010). Results shown in the global maps of Figure 9 are represented in the climatic space in Figure 10. Map pixels were classified according to mean annual temperature and precipitation. For each climate bin the difference between the determination coefficients for NEE vs GPP and TER is reported. Across the whole climate space, IAV retrieved from the MPI-MTE product is mostly controlled by CUP and GPP, although the difference in R^2 in the case of GPP and TER is low. The Jena Inversion on the contrary show climate areas where IAV is CRP driven, especially in intermediate-high temperature classes. Similar results have been reported across several PFT by Yuan et al., (2009) and Ahlstrom et al. (2015) using Fluxnet site data and MTE products. A higher correlation of IAV with GPP rather than with TER in deciduous forests has been reported also by Barr et al. (2002) and Wu et al. (2012). These results suggest that ecosystem fluxes during the CUP, and in particular photosynthesis more than respiration, are consistently controlling the inter-annual variability of NEE at all the spatial scales for both "bottom-up" and "top-down" data products (Janssens et al., 2001; Luyssaert et al., 2007; le Maire et al., 2010; Urbanski et al., 2007; Wohlfahrt et al., 2008a; Wu et al., 2012; Yuan et al., 2009). Temporal variations of photosynthesis and of ecosystem exchange during the carbon uptake period are therefore key to interpret the short-term climate sensitivity of the global carbon cycle.

Biogeosciences Discuss., doi:10.5194/bg-2017-11, 2017
Manuscript under review for journal Biogeosciences
Published: 18 January 2017

4 Conclusions

Patterns and controls of the inter-annual variability of Carbon net ecosystem exchange have been investigated using three different datasets: ecosystem-level data from the FLUXNET database, the MPI-MTE bottom-up statistical upscaling of surface fluxes, and a top-down product based on atmospheric concentration data (Jena CarboScope CO_2 inversion).

The global average of site level IAV_{NEE} (~130 gC $m^{-2}y^{-1}$), computed as the standard deviation of annual NEE, was observed to be almost 6 times the values calculated from the two global products (15 and 20 gC m^{-2} y^{-1} for MPI-MTE and Jena Inversion, respectively). This difference is probably due to the large variability in the spatial scale of point level and gridded products, combined with the scale dependence of the IAV signal, as shown in Fig 4 for the gridded products.

All datasets exhibited smaller IAV at higher latitudes, whereas arid ecosystems showed the largest IAV in the global products. Temperature has the highest correlation with the spatial patterns of IAV, with a positive control at temperature-limited northern ecosystems and a negative control in water-limited zones. Further insights in the sources of IAV have been achieved by exploring the temporal variability of the two gross components: GPP and TER. NEE fluxes during the carbon uptake and carbon release period were used as proxies of GPP and TER, respectively, since the partitioned fluxes were not available for the Jena Inversion. In all three datasets, GPP and NEE_{CUP}, respectively, were shown to control consistently the inter-annual variability NEE across geographical and climate domains, highlighting the fundamental role of photosynthesis in driving the temporal fluctuation of the land sink.

AKNOWLEDGEMENTS

This study was supported by the JRC project AgForCC nr.442. The MCD12C1 product was retrieved from the online Data Pool, courtesy of the NASA EOSDIS Land Processes Distributed Active Archive Center (LP DAAC), USGS/Earth Resources Observation and Science (EROS) Center, Sioux Falls, South Dakota. This work used eddy covariance data acquired and shared by the FLUXNET community, including these networks: AmeriFlux, AfriFlux, AsiaFlux, CarboAfrica, CarboEuropeIP, CarboItaly, CarboMont, ChinaFlux, Fluxnet-Canada, GreenGrass, ICOS, KoFlux, LBA, NECC, OzFlux-TERN, TCOS-Siberia, and USCCC. The FLUXNET eddy covariance data processing and harmonization was carried out by the ICOS Ecosystem Thematic Center, AmeriFlux Management Project and Fluxdata project of FLUXNET, with the support of CDIAC, and the OzFlux, ChinaFlux and AsiaFlux offices.

GPCC Precipitation data provided by the NOAA/OAR/ESRL PSD, Boulder, Colorado, USA, from their Web site at http://www.esrl.noaa.gov/psd/

References

Ahlstrom, A., Raupach, M. R., Schurgers, G., Smith, B., Arneth, A., Jung, M., Reichstein, M., Canadell, J. G., Friedlingstein, P., Jain, a. K., Kato, E., Poulter, B., Sitch, S., Stocker, B. D., Viovy, N., Wang, Y. P., Wiltshire, A., Zaehle, S. and Zeng, N.: The dominant role of semi-arid ecosystems in the trend and variability of the land CO2 sink, Science (80-.)., 348(6237), 895–899, doi:10.1126/science.aaa1668, 2015.

Baker, D. F., Law, R. M., Gurney, K. R., Rayner, P., Peylin, P., Denning, A. S., Bousquet, P., Bruhwiler, L., Chen, Y., Ciais, P., Fung, I. Y., Heimann, M. and Nin, E.: TransCom 3 inversion intercomparison : Impact of transport model errors on the interannual variability of regional CO 2 fluxes , 1988 – 2003, , 20, 1988–2003, doi:10.1029/2004GB002439, 2006.

Bakwin, P., Davis, K., Yi, C. and Wofsy, S.: Regional carbon dioxide fluxes from mixing ratio data, Tellus B, 56, 301–311 [online] Available from: http://onlinelibrary.wiley.com/doi/10.1111/j.1600-0889.2004.00111.x/full (Accessed 9 November 2012), 2004.

Baldocchi, D.: TURNER REVIEW No. 15. "Breathing" of the terrestrial biosphere: Lessons learned from a global network of carbon dioxide flux measurement systems, Aust. J. Bot., 56(1), 1–26, doi:10.1071/BT07151, 2008.

Baldocchi, D., Falge, E., Gu, L., Olson, R., Hollinger, D., Running, S., Anthoni, P., Bernhofer, C., Davis, K., Evans, R., Fuentes, J., Goldstein, A., Katul, G., Law, B., Lee, X., Malhi, Y., Meyers, T., Munger, W., Oechel, W., Paw, K. T., Pilegaard, K., Schmid, H. P., Valentini, R., Verma, S., Vesala, T., Wilson, K. and Wofsy, S.: FLUXNET: A New Tool to

Study the Temporal and Spatial Variability of Ecosystem–Scale Carbon Dioxide, Water Vapor, and Energy Flux Densities, Bull. Am. Meteorol. Soc., 82(11), 2415–2434, doi:10.1175/1520-0477(2001)082<2415:FANTTS>2.3.CO;2, 2001.

Bousquet, P., Peylin, P., Ciais, P., Le Quere, C., Friedlingstein, P. and Tans, P. P.: Regional Changes in Carbon Dioxide Fluxes of Land and Oceans Since 1980, Science (80-.)., 290(5495), 1342–1346, doi:10.1126/science.290.5495.1342, 2000.

Braswell, B., Schimel, D., Linder, E. and Moore, B.: The response of global terrestrial ecosystems to interannual temperature variability, Science (80-.)., 278, 870–872 [online] Available from: http://www.sciencemag.org/content/278/5339/870.short (Accessed 9 November 2012), 1997.

Ciais, P., Reichstein, M., Viovy, N., Granier, a, Ogée, J., Allard, V., Aubinet, M., Buchmann, N., Bernhofer, C., Carrara, a, Chevallier, F., De Noblet, N., Friend, a D., Friedlingstein, P., Grünwald, T., Heinesch, B., Keronen, P., Knohl, a, Krinner, G., Loustau, D., Manca, G., Matteucci, G., Miglietta, F., Ourcival, J. M., Papale, D., Pilegaard, K., Rambal, S., Seufert, G., Soussana, J. F., Sanz, M. J., Schulze, E. D., Vesala, T. and Valentini, R.: Europe-wide reduction in primary productivity caused by the heat and drought in 2003., Nature, 437(7058), 529–533, doi:10.1038/nature03972, 2005.

Cox, P. M., Betts, R. a, Jones, C. D., Spall, S. a and Totterdell, I. J.: Acceleration of global warming due to carbon-cycle feedbacks in a coupled climate model., Nature, 408(6809), 184–187, doi:10.1038/35041539, 2000.

Desai, A. R., Moorcroft, P. R., Bolstad, P. V. and Davis, K. J.: Regional carbon fluxes from an observationally constrained dynamic ecosystem model: Impacts of disturbance, CO2 fertilization, and heterogeneous land cover, J. Geophys. Res. Biogeosciences, 112(1), 1–21, doi:10.1029/2006JG000264, 2007.

Desai, A. R., Noormets, A., Bolstad, P. V., Chen, J., Cook, B. D., Davis, K. J., Euskirchen, E. S., Gough, C., Martin, J. G., Ricciuto, D. M., Schmid, H. P., Tang, J. and Wang, W.: Influence of vegetation and seasonal forcing on carbon dioxide fluxes across the Upper Midwest, USA: Implications for regional scaling, Agric. For. Meteorol., 148(2), 288–308, doi:10.1016/j.agrformet.2007.08.001, 2008.

Desai, A. R., Helliker, B. R., Moorcroft, P. R., Andrews, A. E. and Berry, J. a.: Climatic controls of interannual variability in regional carbon fluxes from top-down and bottom-up perspectives, J. Geophys. Res., 115(G2), G02011, doi:10.1029/2009JG001122, 2010.

Friedl, M. a. and Brodley, C. E.: Decision tree classification of land cover from remotely sensed data, Remote Sens. Environ., 61(3), 399–409, doi:10.1016/S0034-4257(97)00049-7, 1997.

Friedlingstein, P., Houghton, R. a, Marland, G., Hackler, J. L., Boden, T. a, Conway, T. J. and Al, E.: Update on CO 2 emissions, Nat. Geosci., 2010(2007), 6–7, doi:10.1038/ngeo1022, 2010.

Gurney, K. R., Law, R. M., Denning, A. S., Rayner, P. J., Baker, D., Bousquet, P. and Bruhwiler, L.: Towards robust regional estimates of CO 2 sources and sinks using atmospheric transport models, Nature, 415(February), 626–630, 2002.

Heimann, M. and Reichstein, M.: Terrestrial ecosystem carbon dynamics and climate feedbacks., Nature, 451(7176), 289–292, doi:10.1038/nature06591, 2008.

Janssens, I. A., Lankreijer, H., Matteucci, G., Kowalski, A. S., Buchmann, N., Epron, D., Pilegaard, K., Kutsch, W., Longdoz, B., Grünwald, T., Montagnani, L., Dore, S., Rebmann, C., Moors, E. J., Grelle, A., Rannik, Ü., Morgenstern, K., Oltchev, S., Clement, R., Guomundsson, J., Minerbi, S., Berbigier, P., Ibrom, A., Moncrieff, J., Aubinet, M., Bernhofer, C., Jensen, N. O., Vesala, T., Granier, A., Schulze, E. D., Lindroth, A., Dolman, A. J., Jarvis, P. G., Ceulemans, R. and Valentini, R.: Productivity overshadows temperature in determining soil and ecosystem respiration across European forests, Glob. Chang. Biol., 7(3), 269–278, doi:10.1046/j.1365-2486.2001.00412.x, 2001.

Jung, M., Reichstein, M. and Bondeau, a.: Towards global empirical upscaling of FLUXNET eddy covariance observations: validation of a model tree ensemble approach using a biosphere model, Biogeosciences Discuss., 6(3), 5271–5304, doi:10.5194/bgd-6-5271-2009, 2009.

Jung, M., Reichstein, M., Margolis, H. a., Cescatti, A., Richardson, A. D., Arain, M. A., Arneth, A., Bernhofer, C., Bonal, D., Chen, J., Gianelle, D., Gobron, N., Kiely, G., Kutsch, W., Lasslop, G., Law, B. E., Lindroth, A., Merbold, L., Montagnani, L., Moors, E. J., Papale, D., Sottocornola, M., Vaccari, F. and Williams, C.: Global patterns of land-atmosphere fluxes of carbon dioxide, latent heat, and sensible heat derived from eddy covariance, satellite, and meteorological observations, J. Geophys. Res., 116, G00J07, doi:10.1029/2010JG001566, 2011.

Jung, M., Reichstein, M., Schwalm, C. R., Huntingford, C. and Sitch, S.: Compensatory water effects link yearly global land CO2 sink changes to temperature, Nature, (In Press), 2017.

Leuning, R., Raupach, M. R., Coppin, P. a., Cleugh, H. a., Isaac, P., Denmead, O. T., Dunin, F. X., Zegelin, S. and Hacker, J.: Spatial and temporal variations in fluxes of energy, water vapour and carbon dioxide during OASIS 1994 and 1995, Boundary-Layer Meteorol., 110(1), 3–38, doi:10.1023/A:1026028217081, 2004.

Lombardozzi, D., Bonan, G. B. and Nychka, D. W.: The emerging anthropogenic signal in land–atmosphere carbon-cycle coupling, Nat. Clim. Chang., 4(9), 796–800, doi:10.1038/nclimate2323, 2014.

Luyssaert, S., Janssens, I. a., Sulkava, M., Papale, D., Dolman, a. J., Reichstein, M., Hollmén, J., Martin, J. G., Suni, T., Vesala, T., Loustau, D., Law, B. E. and Moors, E. J.: Photosynthesis drives anomalies in net carbon-exchange of pine forests at different latitudes, Glob. Chang. Biol., 13(10), 2110–2127, doi:10.1111/j.1365-2486.2007.01432.x, 2007.

Ma, S., Baldocchi, D. D., Xu, L. and Hehn, T.: Inter-annual variability in carbon dioxide exchange of an oak/grass savanna and open grassland in California, Agric. For. Meteorol., 147(3–4), 157–171, doi:10.1016/j.agrformet.2007.07.008, 2007.

Mahadevan, P., Wofsy, S. C., Matross, D. M., Xiao, X., Dunn, A. L., Lin, J. C., Gerbig, C., Munger, J. W., Chow, V. Y. and Gottlieb, E. W.: A satellite-based biosphere parameterization for net ecosystem CO2 exchange: Vegetation Photosynthesis and Respiration Model (VPRM), Global Biogeochem. Cycles, 22(2), doi:10.1029/2006GB002735, 2008.

le Maire, G., Delpierre, N., Jung, M., Ciais, P., Reichstein, M., Viovy, N., Granier, A., Ibrom, A., Kolari, P., Longdoz, B., Moors, E. J., Pilegaard, K., Rambal, S., Richardson, A. D. and Vesala, T.: Detecting the critical periods that underpin interannual fluctuations in the carbon balance of European forests, J. Geophys. Res., 115, G00H03, doi:10.1029/2009JG001244, 2010.

Marcolla, B., Cescatti, A., Manca, G., Zorer, R., Cavagna, M., Fiora, A., Gianelle, D., Rodeghiero, M., Sottocornola, M. and Zampedri, R.: Climatic controls and ecosystem responses drive the inter-annual variability of the net ecosystem exchange of an alpine meadow, Agric. For. Meteorol., 151(9), 1233–1243, doi:10.1016/j.agrformet.2011.04.015, 2011.

Morgenstern, K., Black, T. A., Humphreys, E. R., Griffis, T. J., Drewitt, G. B., Cai, T., Nesic, Z., Spittlehouse, D. L. and Livingston, N. J.: Sensitivity and uncertainty of the carbon balance of a Pacific Northwest Douglas-fir forest during an El Ni??o/La Ni??a cycle, Agric. For. Meteorol., 123(3–4), 201–219, doi:10.1016/j.agrformet.2003.12.003, 2004.

Pacala, S. W.: Consistent Land- and Atmosphere-Based U.S. Carbon Sink Estimates, Science (80-.)., 292(5525), 2316–2320, doi:10.1126/science.1057320, 2001.

Papale, D. and Valentini, R.: A new assessment of European forests carbon exchanges by eddy fluxes and artificial neural network spatialization, Glob. Chang. Biol., 9(4), 525–535, doi:10.1046/j.1365-2486.2003.00609.x, 2003.

Papale, D., Black, T. A., Carvalhais, N., Cescatti, A., Chen, J., Jung, M., Kiely, G., Lasslop, G., Mahecha, M. D., Margolis, H., Merbold, L., Montagnani, L., Moors, E., Olesen, J. E., Reichstein, M., Tramontana, G., van Gorsel, E., Wohlfahrt, G. and Ráduly, B.: Effect of spatial sampling from European flux towers for estimating carbon and water fluxes with artificial neural networks, J. Geophys. Res. Biogeosciences, 120(10), 1941–1957, doi:10.1002/2015JG002997, 2015.

Polley, H. W., Frank, A. B., Sanabria, J. and Phillips, R. L.: Interannual variability in carbon dioxide fluxes and flux–climate relationships on grazed and ungrazed northern mixed-grass prairie, Glob. Chang. Biol., 14(7), 1620–1632, doi:10.1111/j.1365-2486.2008.01599.x, 2008.

Polley, H. W., Emmerich, W., Bradford, J. a., Sims, P. L., Johnson, D. a., Saliendra, N. Z., Svejcar, T., Angell, R., Frank, A. B., Phillips, R. L., Snyder, K. a. and Morgan, J. a.: Physiological and environmental regulation of interannual variability in CO 2 exchange on rangelands in the western United States, Glob. Chang. Biol., 16(3), 990–1002, doi:10.1111/j.1365-2486.2009.01966.x, 2010.

Poulter, B., Frank, D., Ciais, P., Myneni, R. B., Andela, N., Bi, J., Broquet, G., Canadell, J. G., Chevallier, F., Liu, Y. Y., Running, S. W., Sitch, S. and van der Werf, G. R.: Contribution of semi-arid ecosystems to interannual variability of the global carbon cycle, Nature, 509(7502), 600–603, doi:10.1038/nature13376, 2014.

Le Quere, C., Raupach, M. R., Canadell, J. G., Marland, G., Bopp, L., Ciais, P., Conway, T. J., Doney, S. C., Feely, R. a., Foster, P., Friedlingstein, P., Gurney, K., Houghton, R. a., House, J. I., Huntingford, C., Levy, P. E., Lomas, M. R., Majkut, J., Metzl, N., Ometto, J. P., Peters, G. P., Prentice, I. C., Randerson, J. T., Running, S. W., Sarmiento, J. L., Schuster, U., Sitch, S., Takahashi, T., Viovy, N., Werf, V. Der, Guido, R. and Woodward, F. I.: Trends in the sources and sinks of carbon dioxide, , (November), 1–6, doi:10.1038/ngeo689, 2009.

Le Quéré, C., Peters, G. P., Andres, R. J., Andrew, R. M., Boden, T. a., Ciais, P., Friedlingstein, P., Houghton, R. a., Marland, G., Moriarty, R., Sitch, S., Tans, P., Arneth, a., Arvanitis, a., Bakker, D. C. E., Bopp, L., Canadell, J. G., Chini, L. P., Doney, S. C., Harper, a., Harris, I., House, J. I., Jain, a. K., Jones, S. D., Kato, E., Keeling, R. F., Klein Goldewijk, K., Körtzinger, a., Koven, C., Lefèvre, N., Maignan, F., Omar, a., Ono, T., Park, G. H., Pfeil, B., Poulter, B., Raupach, M. R., Regnier, P., Rödenbeck, C., Saito, S., Schwinger, J., Segschneider, J., Stocker, B. D., Takahashi, T., Tilbrook, B., Van Heuven, S., Viovy, N., Wanninkhof, R., Wiltshire, a. and Zaehle, S.: Global carbon budget 2013, Earth Syst. Sci. Data, 6(1), 235–263, doi:10.5194/essd-6-235-2014, 2014.

Reichstein, M., Papale, D., Valentini, R., Aubinet, M., Bernhofer, C., Knohl, A., Laurila, T., Lindroth, A., Moors, E., Pilegaard, K. and Seufert, G.: Determinants of terrestrial ecosystem carbon balance inferred from European eddy covariance flux sites, Geophys. Res. Lett., 34(1), L01402, doi:10.1029/2006GL027880, 2007.

Richardson, A. D., Hollinger, D. Y., Aber, J. D., Ollinger, S. V. and Braswell, B. H.: Environmental variation is directly responsible for short- but not long-term variation in forest-atmosphere carbon exchange, Glob. Chang. Biol., 13(4), 788–803, doi:10.1111/j.1365-2486.2007.01330.x, 2007.

Rödenbeck, C., Houweling, S., Gloor, M. and Heimann, M.: CO_2 flux history 1982–2001 inferred from atmospheric data using a global inversion of atmospheric transport, Atmos. Chem. Phys., 3(6), 1919–1964, doi:10.5194/acp-3-1919-2003, 2003.

Schneider, U., Becker, A., Finger, P., Meyer-Christoffer, A., Ziese, M. and Rudolf, B.: GPCC's new land surface precipitation climatology based on quality-controlled in situ data and its role in quantifying the global water cycle, Theor. Appl. Climatol., 115(1–2), 15–40, doi:10.1007/s00704-013-0860-x, 2014.

Schultz, M. G., Heil, A., Hoelzemann, J. J., Spessa, A., Thonicke, K., Goldammer, J. G., Held, A. C., Pereira, J. M. C. and van Het Bolscher, M.: Global wildland fire emissions from 1960 to 2000, Global Biogeochem. Cycles, 22(2), 1–17, doi:10.1029/2007GB003031, 2008.

Shao, J., Zhou, X., Luo, Y., Li, B., Aurela, M., Billesbach, D., Blanken, P. D., Bracho, R., Chen, J., Fischer, M., Fu, Y., Gu, L., Han, S., He, Y., Kolb, T., Li, Y., Nagy, Z., Niu, S., Oechel, W. C., Pinter, K., Shi, P., Suyker, A., Torn, M., Varlagin, A., Wang, H., Yan, J., Yu, G. and Zhang, J.: Biotic and climatic controls on interannual variability in carbon fluxes across terrestrial ecosystems, Agric. For. Meteorol., 205, 11–22, doi:10.1016/j.agrformet.2015.02.007, 2015.

Stoy, P. C., Richardson, a. D., Baldocchi, D. D., Katul, G. G., Stanovick, J., Mahecha, M. D., Reichstein, M., Detto, M., Law, B. E., Wohlfahrt, G., Arriga, N., Campos, J., McCaughey, J. H., Montagnani, L., Paw U, K. T., Sevanto, S. and Williams, M.: Biosphere-atmosphere exchange of CO_2 in relation to climate: a cross-biome analysis across multiple time scales, Biogeosciences, 6(10), 2297–2312, doi:10.5194/bg-6-2297-2009, 2009.

Urbanski, S., Barford, C., Wofsy, S., Kucharik, C., Pyle, E., Budney, J., McKain, K., Fitzjarrald, D., Czikowsky, M. and Munger, J. W.: Factors controlling CO 2 exchange on timescales from hourly to decadal at Harvard Forest, J. Geophys. Res., 112(G2), G02020, doi:10.1029/2006JG000293, 2007.

Valentini, R., Matteucci, G., Dolman, a J., Schulze, E. D., Rebmann, C., Moors, E. J., Granier, a, Gross, P., Jensen, N. O., Pilegaard, K., Lindroth, a, Grelle, a, Bernhofer, C., Grünwald, T., Aubinet, M., Ceulemans, R., Kowalski, a S., Vesala, T., Rannik, U., Berbigier, P., Loustau, D., Gudmundsson, J., Thorgeirsson, H., Ibrom, a, Morgenstern, K. and Clement, R.: Respiration as the main determinant of carbon balance in European forests., Nature, 404(6780), 861–865, doi:10.1038/35009084, 2000.

Van Der Werf, G. R., Randerson, J. T., Giglio, L., Collatz, G. J., Mu, M., Kasibhatla, P. S., Morton, D. C., Defries, R. S., Jin, Y. and Van Leeuwen, T. T.: Global fire emissions and the contribution of deforestation, savanna, forest, agricultural, and peat fires (1997-2009), Atmos. Chem. Phys., 10(23), 11707–11735, doi:10.5194/acp-10-11707-2010, 2010.

Wohlfahrt, G., Hammerle, A., Haslwanter, A., Bahn, M., Tappeiner, U. and Cernusca, A.: Seasonal and inter-annual variability of the net ecosystem CO2 exchange of a temperate mountain grassland: effects of climate and management., J. Geophys. Res. Atmos. JGR, 113(D8), doi:10.1029/2007jd009286, 2008a.

Wohlfahrt, G., Hammerle, A., Haslwanter, A., Bahn, M., Tappeiner, U. and Cernusca, A.: Seasonal and inter-annual variability of the net ecosystem CO 2 exchange of a temperate mountain grassland: Effects of weather and management, J. Geophys. Res., 113(D8), D08110, doi:10.1029/2007JD009286, 2008b.

Wu, J., van der Linden, L., Lasslop, G., Carvalhais, N., Pilegaard, K., Beier, C. and Ibrom, A.: Effects of climate variability and functional changes on the interannual variation of the carbon balance in a temperate deciduous forest, Biogeosciences, 9(1), 13–28, doi:10.5194/bg-9-13-2012, 2012.

Yuan, W., Luo, Y., Richardson, A. D., Oren, R., Luyssaert, S., Janssens, I. a., Ceulemans, R., Zhou, X., Grunwald, T., Aubinet, M., Berhofer, C., Baldocchi, D. D., Chen, J., Dunn, A. L., Deforest, J. L., Dragoni, D., Goldstein, A. H., Moors, E., William Munger, J., Monson, R. K., Suyker, A. E., Starr, G., Scott, R. L., Tenhunen, J., Verma, S. B., Vesala, T. and Wofsy, S. C.: Latitudinal patterns of magnitude and interannual variability in net ecosystem exchange regulated by biological and environmental variables, Glob. Chang. Biol., 15(12), 2905–2920, doi:10.1111/j.1365-2486.2009.01870.x, 2009.

Zhao, M. and Running, S. W.: Drought-induced reduction in global terrestrial net primary production from 2000 through 2009., Science, 329(5994), 940–3, doi:10.1126/science.1192666, 2010.

Biogeosciences Discuss., doi:10.5194/bg-2017-11, 2017
Manuscript under review for journal Biogeosciences
Published: 18 January 2017

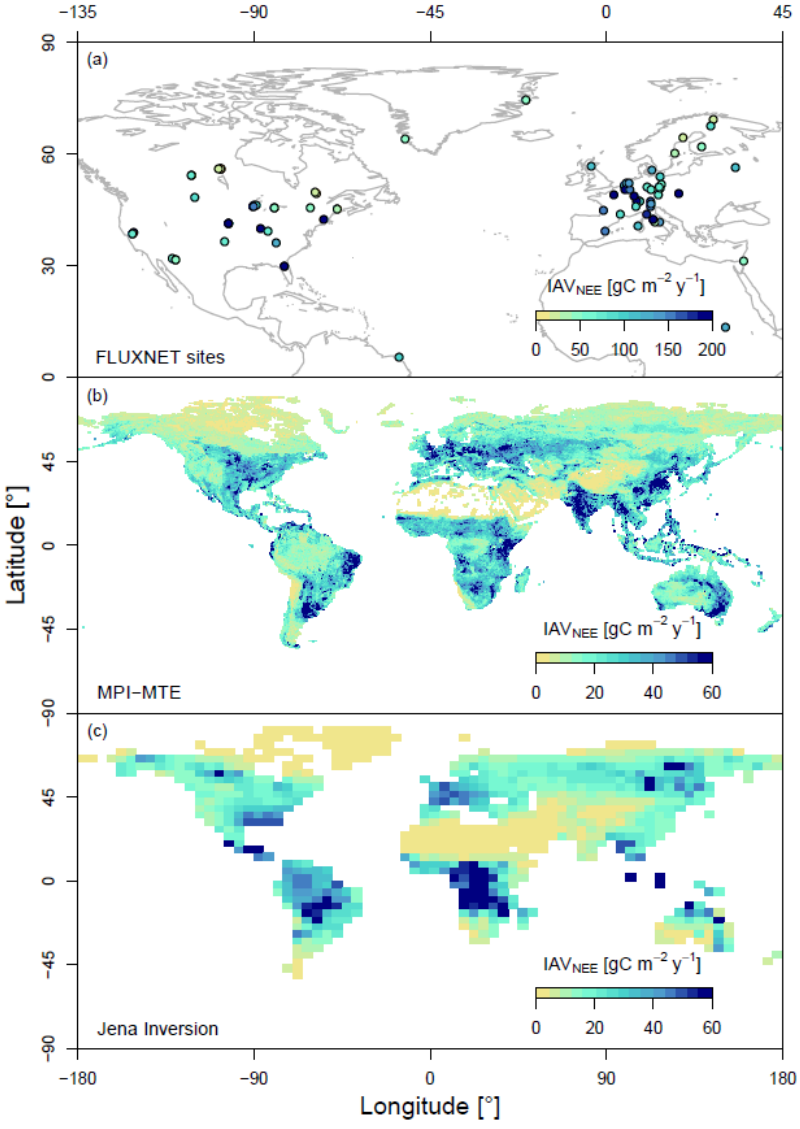

485 **Figure 1: Spatial distribution of NEE standard deviation used as a measure of inter-annual variability (IAV$_{NEE}$). Results are reported for a) Fluxnet sites with at least 5 years of observations, b) for the MPI-MTE NEE product and c) Jena Inversion product s81_v3.6.**

Biogeosciences Discuss., doi:10.5194/bg-2017-11, 2017
Manuscript under review for journal Biogeosciences
Published: 18 January 2017

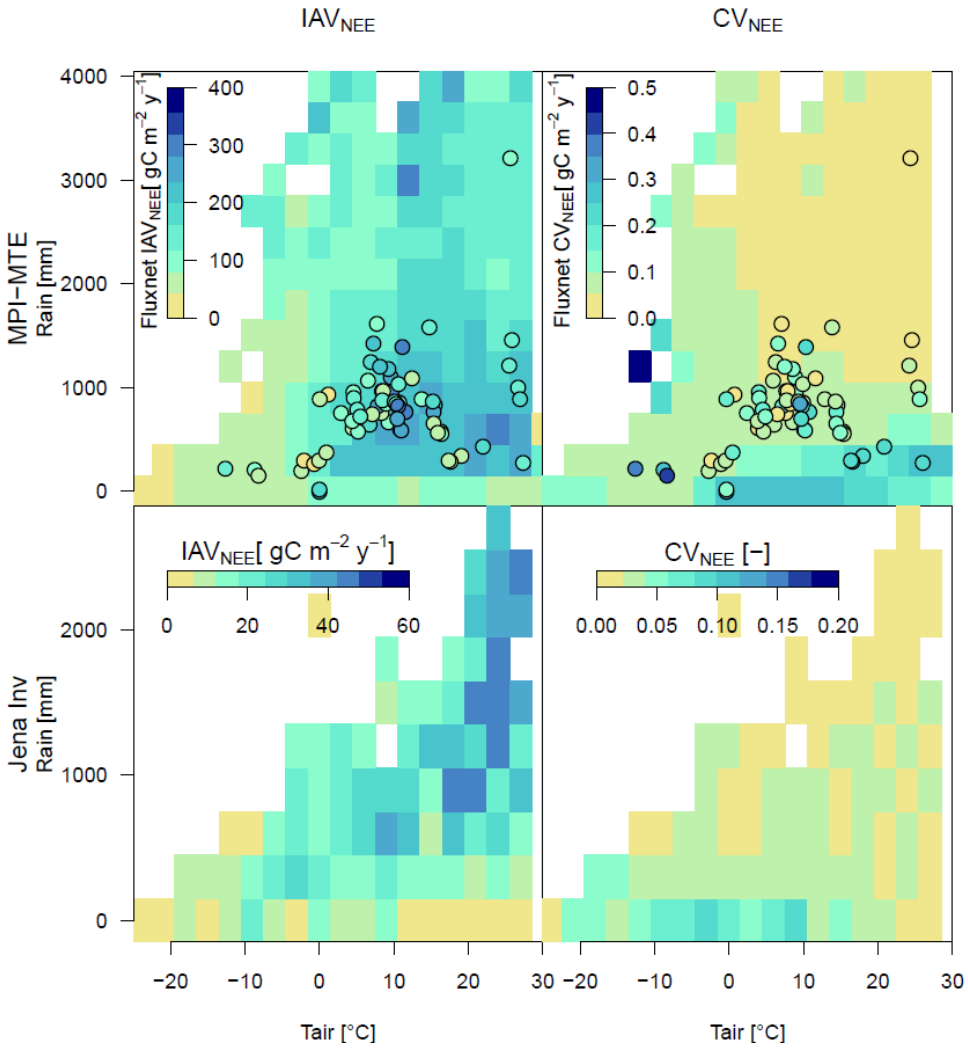

Figure 2: IAV$_{NEE}$ (left panels) and normalized IAV$_{NEE}$ (CV$_{NEE}$, right panels) plotted in a Temperature-Precipitation space, for MPI-MTE (top panels) and Jena Inversion (bottom panels). Dots represent Fluxnet site values.

Biogeosciences Discuss., doi:10.5194/bg-2017-11, 2017
Manuscript under review for journal Biogeosciences
Published: 18 January 2017

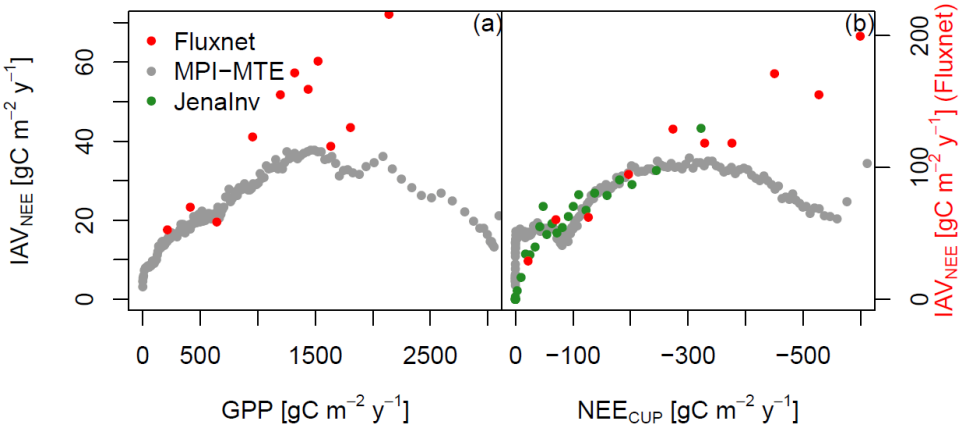

495

Figure 3: Dependency of standard deviation of NEE on GPP and NEE_{CUP} . Results are reported for Fluxnet sites (red dots, different y scale on the right), for the MPI-MTE NEE (black dots) and Jena Inversion product (green dots)

Biogeosciences Discuss., doi:10.5194/bg-2017-11, 2017
Manuscript under review for journal Biogeosciences
Published: 18 January 2017

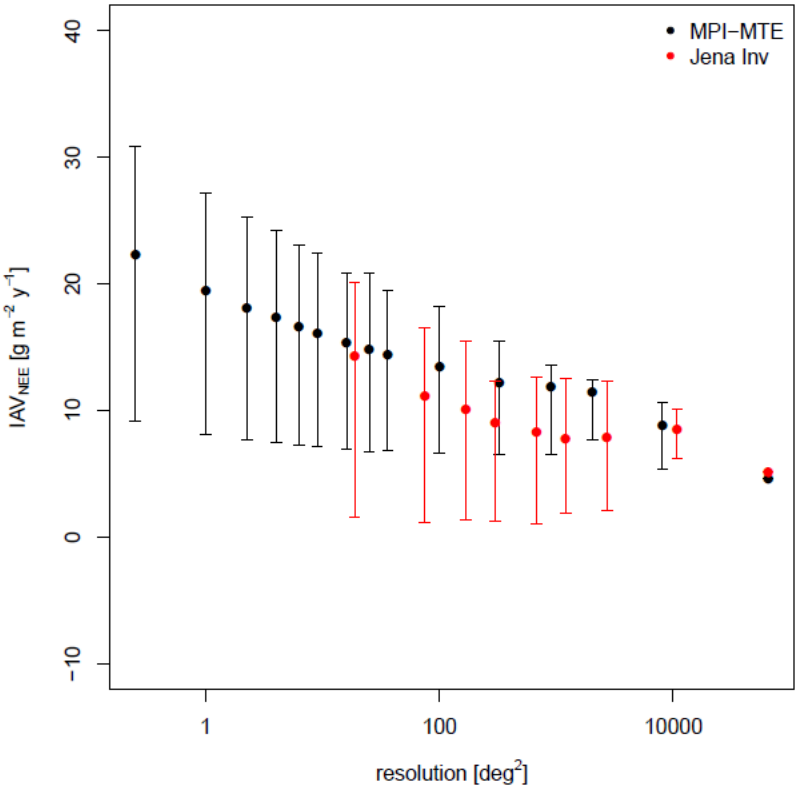

500

Figure 4: Dependence of IAV_{NEE} on map resolution for MPI-MTE (black dots) and Jena Inversion (red dots). Error bars represent the 25% and 75% quantiles of the IAV in the aggregated pixels.

Biogeosciences Discuss., doi:10.5194/bg-2017-11, 2017
Manuscript under review for journal Biogeosciences
Published: 18 January 2017

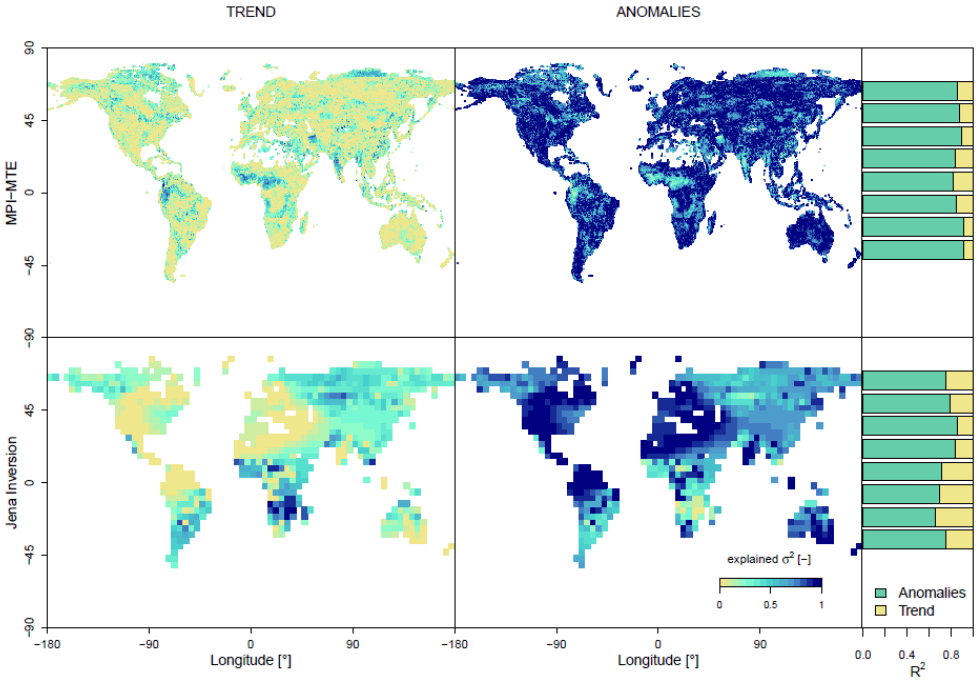

Figure 5: Maps of the fraction of NEE variance explained by temporal trends and anomalies for MPI-MTE NEE and Jena Inversion; latitudinal band (15°) averages of the fractions are reported in the bar plots.

Biogeosciences Discuss., doi:10.5194/bg-2017-11, 2017
Manuscript under review for journal Biogeosciences
Published: 18 January 2017

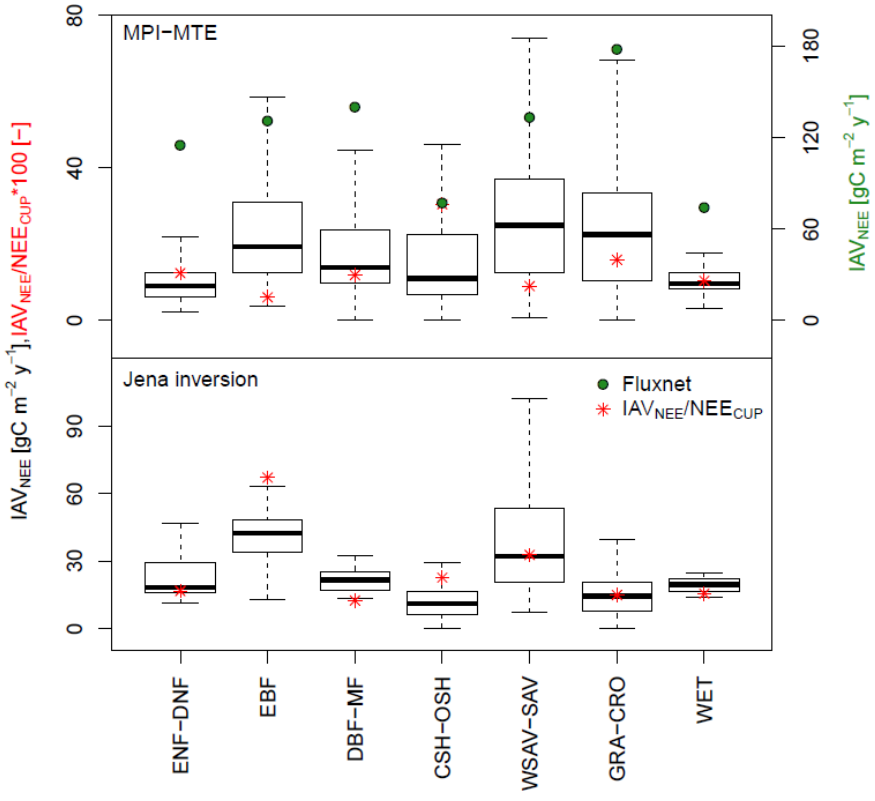

Figure 6: Boxplot of NEE standard deviation averaged in PFT classes for MPI-MTE NEE and Jena Inversion, green dots represent observations at Fluxnet sites (different y scale on the right).

515

Biogeosciences Discuss., doi:10.5194/bg-2017-11, 2017
Manuscript under review for journal Biogeosciences
Published: 18 January 2017

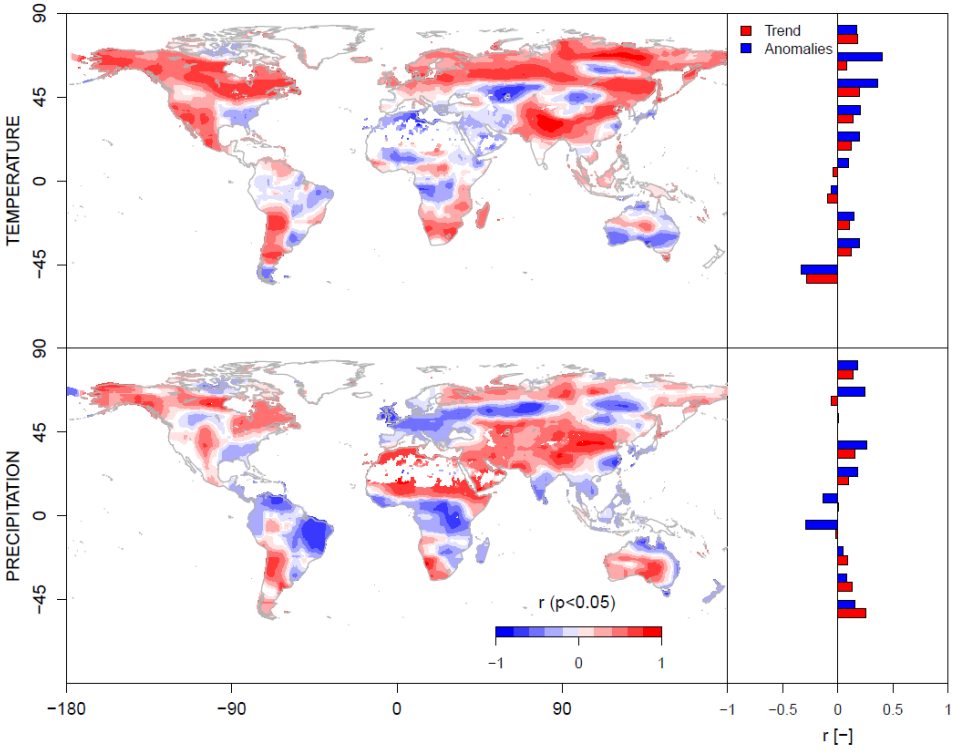

520 **Figure 7: Climatic drivers of the spatial variability of NEE standard deviation. The left panels show maps of the spatial correlation coefficients (within moving spatial windows of 15°x11.5°) of interannual NEE amplitude versus time-mean temperature and precipitation for the bottom up product MPI-MTE. Pixels with non-significant correlation are left white. The barplots on the right show latitudinal averages of the correlation coefficients of NEE trend and anomalies versus temperature and precipitation.**

525

Biogeosciences Discuss., doi:10.5194/bg-2017-11, 2017
Manuscript under review for journal Biogeosciences
Published: 18 January 2017

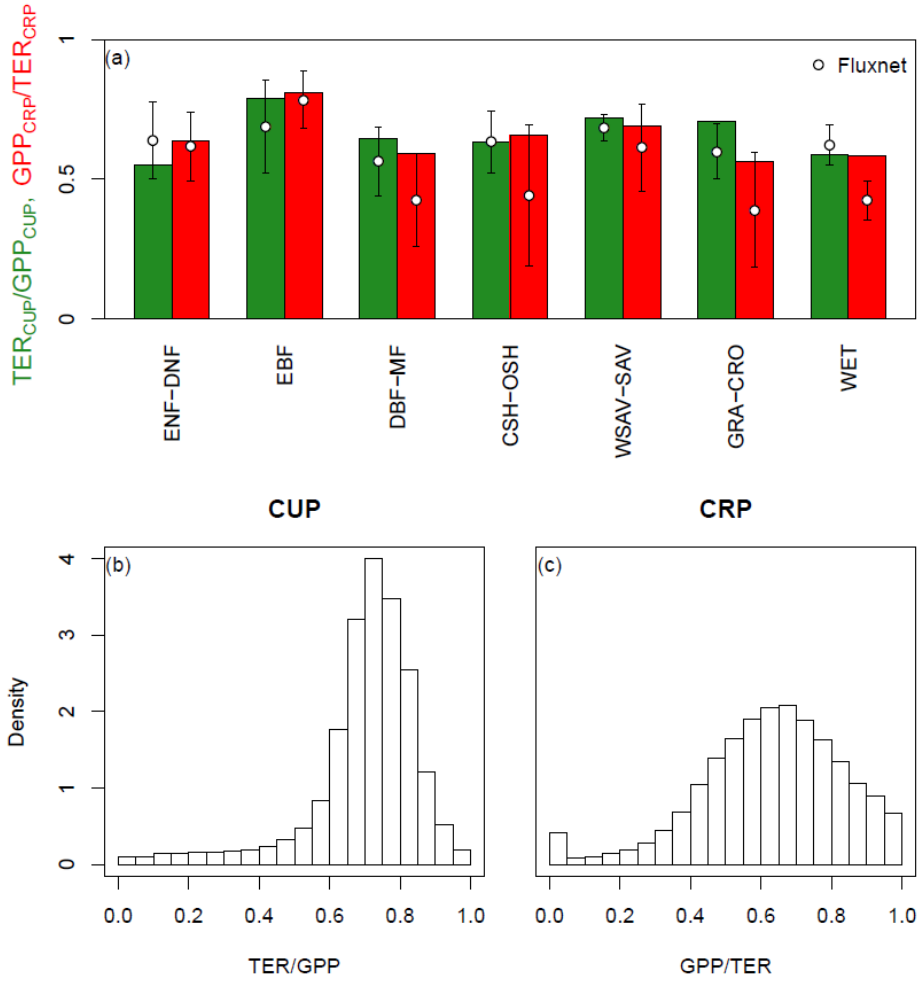

Figure 8: Bar plot of the ratio TER/GPP for the Carbon Uptake Period (CUP) and of the ratio GPP/TER during the Carbon Release Period (CRP), these values were calculated for the MPI-MTE product, dots refer to Fluxnet sites. Averages of yearly values are represented together with their standard deviation. The global frequency distributions of the ratios obtained from the MPI-MTE product are reported in the histograms at the bottom.

Biogeosciences Discuss., doi:10.5194/bg-2017-11, 2017
Manuscript under review for journal Biogeosciences
Published: 18 January 2017

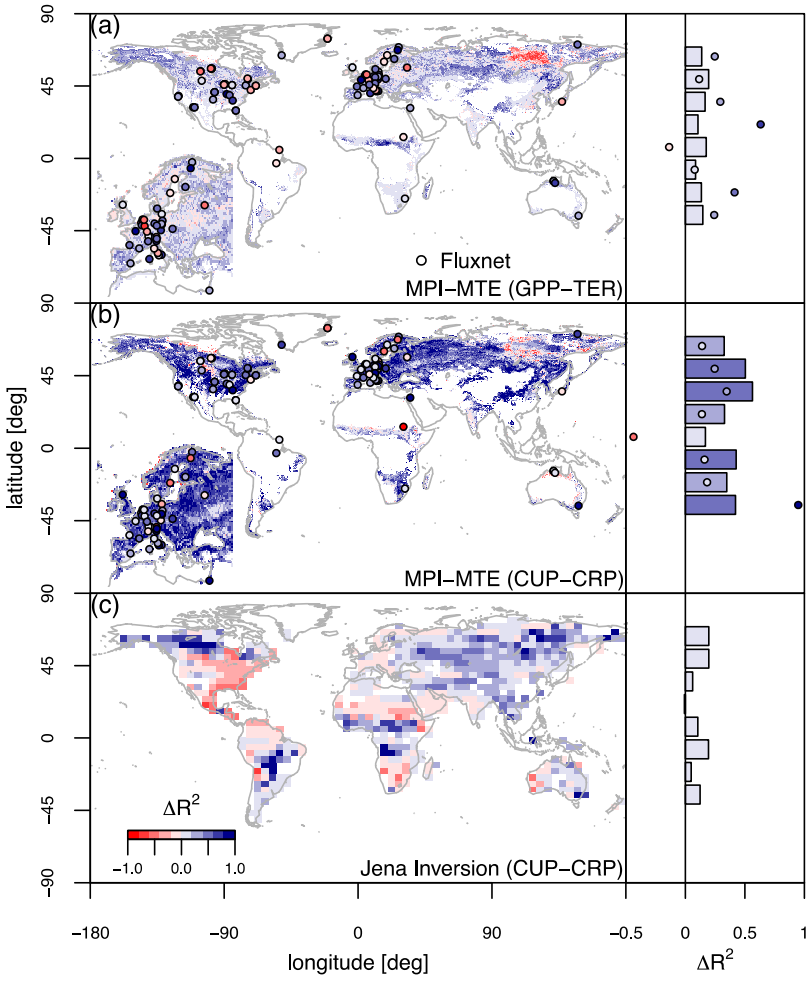

535

Figure 9: Control on IAV by GPP-TER and Carbon Uptake Period (CUP) - Carbon Release Period (CRP), expressed as the difference of the determination coefficients for Fluxnet sites with at least 5 years of observations (dots), MPI-MTE NEE and Jena Inversion. Latitudinal averages are reported for latitudinal classes of 15 degrees. Inset maps show an enlarged plot of Europe.

540

Biogeosciences Discuss., doi:10.5194/bg-2017-11, 2017
Manuscript under review for journal Biogeosciences
Published: 18 January 2017

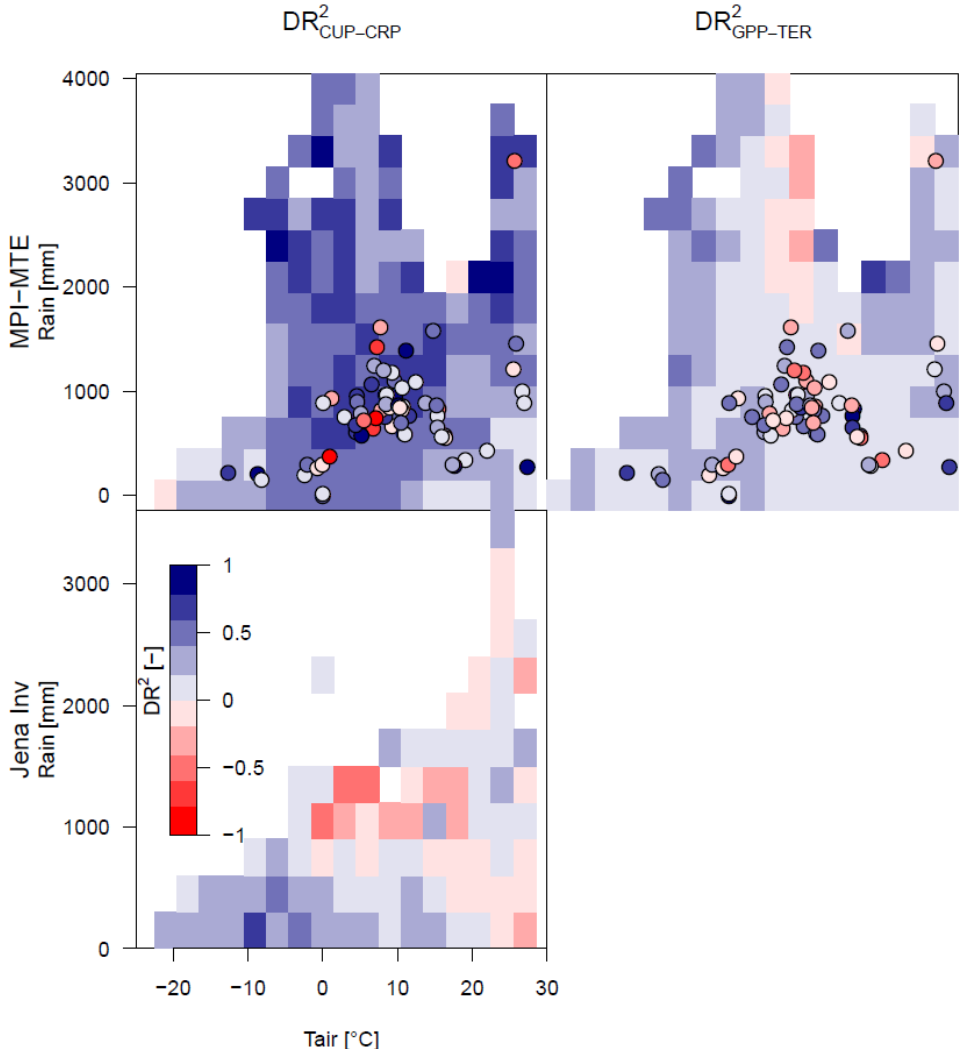

Figure 10: Control on IAV by GPP-TER and Carbon Uptake Period (CUP) - Carbon Release Period (CRP), expressed as the difference of the determination coefficients plotted in a Temperature Precipitation space. The two top panels refers to MPI-MTE while the bottom panel to Jena Inversion, dots refer to Fluxnet sites.